Journal of Photochemistry and Photobiology A: Chemistry 269 (2013) 49–58

Contents lists available at ScienceDirect

Journal of Photochemistry and Photobiology A: Chemistry

journal homepage: www.elsevier.com/locate/jphotochem

Effectively dispersed europium oxide dopants in TiO_2 aerogel supports for enhanced photocatalytic pollutant degradation

Harrison S. Kibombo[a], Amanda S. Weber[b], Chia-Ming Wu[a], Krishna Reddy Raghupathi[c], Ranjit T. Koodali[a,*]

[a] Department of Chemistry, University of South Dakota, Vermillion, SD 57069, USA
[b] Department of Chemistry, University of California, Irvine, Irvine, CA 92697, USA
[c] Department of Chemistry, University of Massachusetts, Amherst, MA 01003, USA

ARTICLE INFO

Article history:
Received 12 June 2013
Received in revised form 8 July 2013
Accepted 10 July 2013
Available online 23 July 2013

Keywords:
Hydroxyl radicals
Aerogels
Europium oxide
Eu-TiO_2
Supercritical drying

ABSTRACT

The influence of supercritical drying and the europium oxide content on the physicochemical properties and the resultant photocatalytic activity of Eu-TiO_2 aerogels for the degradation of salicylic acid were explored for the first time. It was demonstrated that the efficiencies might be influenced by a combination of factors such as enhanced adsorption, presence of trap states, and/or suppression of rutile phase formation. The well dispersed europium oxide dopants may act as trap states. A subsequent enhancement of charge separation avails electrons for oxygen attack to form superoxide ions, from which $^{\bullet}OH$ radicals can be generated, and are postulated to be primary contributors toward the degradation efficiencies in this study.

1. Introduction

Air, land, and water pollution is one of the main environmental concerns facing our world today that is taking precedence in the natural resource sustainability debate. The use of contaminated ground water, for example, is a likely source of human contact with potentially toxic organic pollutants such as phenols, aromatic carboxylic acids, dyes, surfactants, pesticides, pharmaceutical waste, and endocrine disrupting compounds (EDCs). Traditional methods of water treatment (such as adsorption, filtration, and ozonation) are still limited because they are energy intensive, tedious, may produce toxic by-products, and require several elaborate steps for the remediation process. One emerging approach to mitigate these challenges has been the use of photocatalysis, an advanced oxidation process (AOP) that promises the use of abundant sunlight for the complete mineralization of toxic pollutants.

Titanium dioxide (TiO_2) is a popular photocatalyst of choice due to its unique physicochemical properties, high mechanical and thermal stability, ease of synthesis, relatively low cost, and high degradation efficiencies [1]. The anatase polymorph of TiO_2 has been widely preferred for various heterogeneous reactions and has exhibited enhanced activities compared to the brookite or the rutile forms. However, a major drawback to TiO_2 is that it absorbs light only in the UV region, which accounts for less than 5% of the solar radiation that reaches the Earth's surface.

Current research efforts are focused on more practical and widespread use of the photocatalyst and its derivatives for detoxification and other light driven applications by examining means of extending the response of the titania into the visible region so as to utilize light from larger portions of the electromagnetic spectrum. Another approach has been to maximize the activity of TiO_2 under UV irradiation by utilizing preparation methods, which optimize structural and electronic properties that are considered relevant for mineralization processes. This work attempts to address the latter approach by exploring the role of incorporating rare-earth ions/oxides such as lanthanides in the titania matrix. Such ions have been proposed to form strong interactions *via* their *f*-orbitals with functional groups, which increases the propensity to adsorb more pollutant molecules at the surface of the photocatalyst, and thus enhance photocatalytic efficiency of titania [2–4].

Here, different loadings of Eu-TiO_2 were prepared using the sol–gel method, and the resulting wet gels were dried under supercritical conditions to form aerogel powders. This drying method was preferred because solvent removal in the supercritical state minimizes the formation of the liquid–vapor meniscus, and subsequently minimizes the likelihood of occurrence of the pore collapse

* Corresponding author. Tel.: +1 605 677 6189; fax: +1 605 677 6397.
E-mail addresses: Ranjit.Koodali@usd.edu, ktranjit@gmail.com (R.T. Koodali).

1010-6030/$ – see front matter © 2013 Elsevier B.V. All rights reserved.
http://dx.doi.org/10.1016/j.jphotochem.2013.07.006

phenomenon. This approach promises materials of high porosities, high surface areas, low density, and relatively low agglomeration [5–7]. In this study, the role of high temperature supercritical drying (HTSCD) on the dispersion of the europium ions in the anatase support for the improvement of the photocatalytic degradation of salicylic acid was investigated. HTSCD involves use of hot alcohol solvents in the supercritical state, and is attractive because it shortens the processing time from several days to a few hours [8], and promises thermodynamically stabilized materials of enhanced crystallinity [7,9–11].

Previous studies have primarily explored the change in electronic and physicochemical properties due the modification of the titania nanoparticles using europium ions [12–21], and some reports have demonstrated their application for organic pollutant degradation [2,22–36]. However, the preparation methods influence the structural properties as well as the photocatalyst efficiencies as a result. A comprehensive literature search reveals only one report that investigates the role of aerogel synthesis and it simply addresses the effect of dopant concentration on the luminescence properties [37]. The demonstration of the efficacy of Eu-TiO_2 aerogel based photocatalysts for organic pollutant degradation in aqueous phase is still missing in the literature and thus this work is the first attempt in using supercritical drying method to prepare europium oxide dopants in titania aerogel materials. The enhancement in the photocatalytic activity on modification with rare earth metal ions/oxides such as europium ions/oxides have been ascribed to a combination of several factors that include: (1) enhanced adsorption of the organics by the formation of Lewis acid–base complexes [27]; (2) the prolonged separation of electrons and holes facilitated by the formation of defects (Ti^{3+}) and oxygen vacancies on the surface can act as trap states (3); the enhancement of surface hydroxyl groups (arising from the charge imbalance in the event of isomorphic substitution of Eu^{3+} for Ti^{4+}) that react with the holes to form hydroxyl radicals and facilitate the photocatalytic reaction; (4) the inhibition of the anatase to rutile phase transformation, which permits the more negative conduction band edge and the open structure of the anatase phase to facilitate higher photoactivity in comparison to the rutile phase; and (5) the ability of europium ions to trap electrons and minimize charge carrier recombination under UV irradiation [38].

Thus, this manuscript presents the *first* report of the preparation of surfactant template free Eu-TiO_2 aerogel photocatalysts obtained under HTSCD that is utilized for the degradation of salicylic acid as a probe molecule. In addition, a probe into the overriding physicochemical factors that influence the photocatalytic activity is attempted by incorporating scavenging experiments. The resultant aerogel photocatalysts were also characterized by powder X-ray diffraction, nitrogen physisorption, electron microscopy, X-ray photoelectron microscopy, photoluminescence, and diffuse reflectance spectroscopy.

2. Experimental

2.1. Materials

The following chemicals were purchased from Acros Chemical Company, USA; toluene (C_7H_8, ACS grade), methanol (CH_3OH, 99.8%), titanium isopropoxide ($Ti[OCH(CH_3)_2]_4$, 98+ %), europium nitrate ($Eu(NO_3)\cdot 6H_2O$), salicylic acid ($C_7H_6O_3$, ACS grade), sodium hydroxide (NaOH), and terephthalic acid (TPA, ACS grade) were used as received. The deionized water was obtained from a NANO ultrapure water system manufactured by Barnstead International, USA.

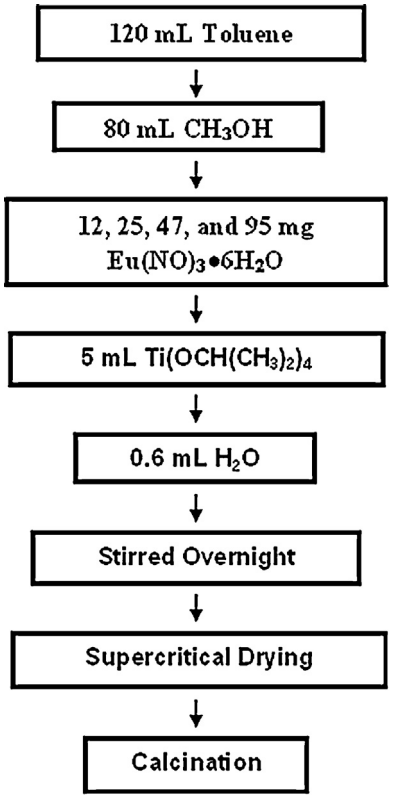

Scheme 1. Schematic illustration of the synthetic procedure for the preparation of Eu-TiO_2 aerogel photocatalysts.

2.2. Synthesis of the photocatalysts

2.2.1. Preparation of europium oxide doped TiO_2 aerogels

Europium oxide doped titania aerogels of our different molar ratios of Eu/Ti were synthesized using the sol–gel method, prior to high temperature supercritical drying, and the preparation procedure is summarized in Scheme 1. 120 mL of toluene was mixed with 80 mL of methanol. An appropriate amount of europium nitrate and then 5 mL of titanium isopropoxide was added to the solvent mixture under a stirring rate of 300 rpm. Finally, 0.6 mL of deionized water was added drop-wise to initiate the hydrolysis reaction. Stirring was continued overnight (~12 h) at room temperature to provide sufficient time for the suspension to gel. The gel was transferred to a glass liner (600 mL capacity) and the autoclave (Parr Model 5500 high pressure compact stirred reactor with temperature controller 4836) was assembled, sealed and nitrogen gas was admitted into the chamber at about 100 psi. Heating was carried out at a rate of 1 °C/min until 265 °C. This was chosen as the supercritical temperature for the methanol and toluene solvents based on previous reports that promise good results under similar conditions, and the necessity to avoid any thermal decomposition of the solvent [39]. The pressure inside the autoclave gradually increases up to 1200 psi as the supercritical temperature is achieved. Such supercritical conditions were maintained for at least 15 min, and the solvent was rapidly removed thereafter by opening the outlet valve to vent. The autoclave was then allowed to cool to room temperature and disassembled. A light yellow colored aerogel powder was obtained, and was found to be amorphous at this stage. Thus, it was ground into a finer powder and calcinated at 550 °C for 6 h in a tubular furnace (Thermolyne Barnstead Model 21100) in order to impart crystallinity. A color change from yellow to a white europium doped titania (Eu-TiO_2) was observed after calcination, and subsequently, the resultant aerogel powders were

Table 1
Phase composition, unit cell parameters, unit cell volume, and crystallite sizes of Eu^{3+} doped TiO_2 materials determined from the XRD analysis. The value preceding Eu-TiO_2 represents the wt.% of Eu_2O_3 loaded into the TiO_2.

Aerogel	Crystal phase	Unit cell parameters (nm)		Unit cell volume $(nm)^3$	Crystallite size (nm)
		a and *b*	*c*		
TiO_2	Anatase	0.3782	0.958	13.781	12.0 ± 2.0
0.72-Eu-TiO_2	Anatase	0.3783	0.949	13.591	10.6 ± 2.0
1.48-Eu-TiO_2	Anatase	0.3784	0.951	13.609	9.9 ± 2.0
2.71-Eu-TiO_2	Anatase	0.3788	0.946	13.581	9.1 ± 2.0
5.30-Eu-TiO_2	Anatase	0.3785	0.951	13.622	10.7 ± 2.0

characterized in addition to photocatalytic efficiency evaluation. Four different europium oxide doped titania materials were prepared and the number (0.72, 1.48, 2.71, and 5.30) in the sample label refer to the weight percent of europium oxide in the final calcined material determined by ICP-MS technique.

2.3. Characterization techniques

The europium oxide containing TiO_2 nanomaterials were characterized by several techniques as detailed in this section of the manuscript. Information on the nature of the phase of the photocatalysts was determined by using powder X-ray diffraction (XRD) from a Rigaku Ultima IV diffractometer. The diffraction patterns were obtained at room temperature using Ni filtered CuK_α (λ = 1.5418 Å) radiation as an X-ray source. The diffractometer was operated at a voltage of 44 kV and a current of 40 mA. The diffraction patterns was measured from 20 to 74° (2θ) with the following parameters: a step size of 0.02°, divergence and scattering slit of 2°, receiving slit of 0.45 mm, and divergence height limiting slit of 10 mm. The diffractograms obtained were analyzed by using PDLX software provided by Rigaku, from which we can identify the crystal phases formed, the unit cell parameters, the crystallinity of the material, and the crystallite size. Prior to running the XRD analysis, the samples were dried overnight in an oven at 80 ± 10 °C.

The textural properties (such as surface area, pore volume, and pore size) were estimated by nitrogen physisorption analysis at 77 K using a Nova 2200*e* surface area and pore size analyzer. Prior to N_2 adsorption, the samples were degassed extensively at 100 °C for several hours to ensure that any water molecules or gases adsorbed in the pores were expelled. The Brunauer–Emmett–Teller (BET) method was used to determine the surface area from the N_2 adsorption isotherm within the relative pressure (P/P_0) range of 0.05–0.30. The pore volume was calculated at the highest relative pressure of (P/P_0) ~ 0.99. The pore size distribution was determined using the Barrett–Joyner–Halenda (BJH) method that was applied to data from the desorption isotherms.

Transmission electron microscopy (TEM) was used to obtain information about the morphology (size and shape) of the aerogel materials. The samples were prepared for analysis by suspending a few mg of the nanomaterial powder in ethanol, and sonicated to form a uniform suspension. Then, a few drops of this suspension were carefully placed on a carbon-coated copper grid (200 mesh size). The grid was allowed to dry overnight before conducting the TEM analysis. Microimages were acquired from a Hitachi (H7000FA) instrument operating at a voltage of 100 kV.

Scanning electron microscopy (SEM) was also used to examine the microscopic features such as surface properties, shape and texture of the nanomaterials. The samples were placed on a double side carbon paper that was adhered to an alumina mount in order to prevent charging effect prior to imaging on a Zeiss Supra (40 VP FESEM), which was operated at 4 keV. The working distance from the microscope lens was about 6 mm. The condenser aperture was set at 20 μm, and a standard secondary electron detector was used for acquiring the high resolution SEM images.

Diffuse reflectance spectroscopy (DRS) was used to estimate the band gap energy of the Eu-TiO_2 aerogels. The spectra were obtained by using a Cary 100 Bio Spectrophotometer that was equipped with a DR accessory. All data were taken at room temperature in the wavelength range of 190–600 nm. The band gap energy (E_g^{eff} (eV)) was determined by a linear extrapolation of the wavelength at which the absorbance was equal to zero. This wavelength (λ_g^{eff}) estimated from a graphical plot was then used in the equation: $E_g^{eff}(eV) = 1239.6/\lambda(nm)$ to estimate the band gap of the photocatalysts [40].

The X-ray photoelectron spectroscopic (XPS) measurement was carried out using a custom-designed Kratos Axis Ultra instrument. The samples were placed in a surface analysis chamber under monochromatic radiation at 1486.6 eV from an aluminum K_α source using a 500 mm Rowland circle silicon single crystal monochromator. The X-ray gun was operated with a current at 15 mA and at an accelerating voltage of 15 kV. Low energy electrons were used for the charge compensation to neutralize the samples, after which they were transferred to the indium foil and mounted on the copper stub. High resolution spectra were acquired in the region of interest using the following parameters: 20–40 eV energy windows, pass energy of 20 eV, step size of 0.1 eV, and dwell time of 1000 ms. The absolute energy scale was calibrated to the Cu $2p_{2/3}$ peak binding energy of 932.6 eV using an etched copper plate. All spectra were calibrated using C 1s peak at 284.6 eV, and a Tougaard-type background was subtracted from each spectrum.

2.4. Photocatalytic studies

A calibration plot was derived from a serial dilution of a 1×10^{-3} M stock solution of salicylic acid. 7 ± 0.5 mg of TiO_2 or Eu-TiO_2 photocatalyst were suspended in 3 mL of 2×10^{-4} M salicylic acid were in a quartz cuvette (3.5 mL capacity, Sigma–Aldrich, 10 mm light path). The suspension was stirred for 30 min in the dark under oxygen purging. After the 30 min period of equilibration (to establish adsorption–desorption equilibria), the suspension was irradiated with a 1000 W Xe-Hg lamp (Newport) power source attached to a water circulation bath in order to filter IR radiation. A Pyrex filter (with transmission in the 350–550 nm range) was used for the photocatalytic studies. All samples were irradiated for specific amounts of time *i.e.* 30, 45, and 60 min, and the suspension was centrifuged to remove the suspended photocatalyst particulates. The UV–vis (Cary 100 Bio spectrophotometer) spectra of salicylic acid were then recorded and exhibited a peak at λ = 296 nm, which is monitored and used in conjunction with the calibration plot to estimate the concentration remaining after the photocatalytic reaction.

Additional experiments were carried in the presence of N_2 flow (absence of oxygen) in order to eliminate molecular O_2, with a purpose of determined the species that play a significant role in the salicylic acid degradation under our experimental conditions. In addition, the contribution of hydroxyl radicals (•OH) on the photocatalytic reaction was studied by applying the fluorescence technique that detects the amount of •OH formed on illuminated

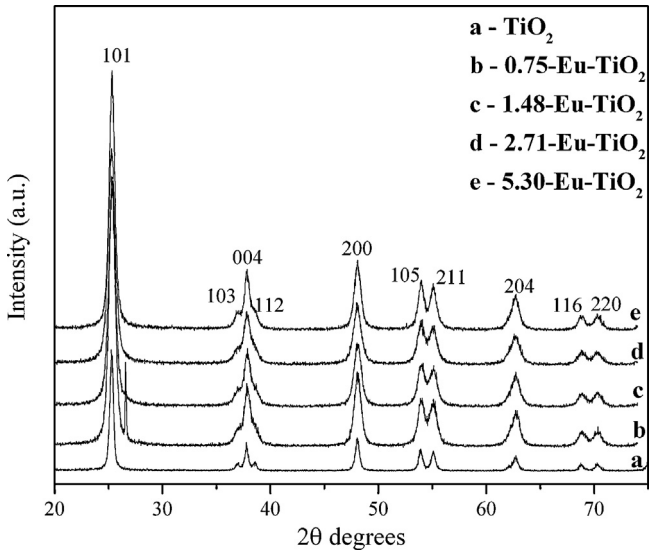

Fig. 1. XRD patterns of Eu-TiO_2 aerogels. The value preceding Eu-TiO_2 represents the wt.% of Eu_2O_3 loaded into the TiO_2.

Eu-TiO_2 aerogel surfaces. Terephthalic acid (TPA) was used as a chemical trap for the •OH radicals, which are known to react readily with TPA to produce highly fluorescent 2-hydroxyterephthalic acid (2-HTPA). In this reaction, 20 mg of photocatalyst were added to 50 mL of 5×10^{-4} M TPA solution in 2×10^{-3} M NaOH, prior to UV irradiation. 3 mL aliquots were drawn every 20 min for a duration of 80 min, filtered through a 0.45 μm Millipore filter membrane, and analyzed using Flouromax-4 (JY Horiba) fluorometer. The fluorescence emission intensity of the 2-hydroxyterephthalic acid produced a peak at 425 nm after excitation at 315 nm. The intensity of the peak at 425 nm is expected to be proportional to the amount of •OH formed.

2.5. Dark adsorption

Adsorption studies were performed in the dark for all samples in order to investigate the relationships between photocatalytic degradation and the amount of organics that adsorb onto the surface in solution. About 10 mg of the Eu-TiO_2 photocatalysts were suspended in 10 mL of 2×10^{-4} M solution of salicylic acid in an amber glass tinted bottle. Each bottle was wrapped with aluminum foil to prevent absorption of ambient light. The suspensions were kept in the dark and stirred at 300 rpm for 6 h, centrifuged 3–5 times in order to remove the solid particulates completely. UV–vis spectra were then recorded to determine the amount of salicylic acid that was adsorbed onto the aerogel particles.

3. Results and discussion

3.1. Powder X-ray diffraction studies

XRD provides information pertaining to the identity of the phase, crystallinity and allows for an estimation of the crystallite sizes of the titania phase. Fig. 1 displays the X-ray diffraction patterns for the Eu-TiO_2 aerogels prepared in this study. The photocatalysts exhibit sharp peaks of high diffraction contrast that is characteristic of small crystallites of the anatase crystal phase of TiO_2 ($I4_1/amd$, JCPDS 21-1272). Our results indicate that the anatase was the most predominant phase, and was preserved at calcination temperatures as high as 550 °C. The absence of peaks due to Eu_2O_3 phases in the XRD patterns suggests that the sol–gel method used for preparation led to the formation of a highly uniform, homogeneous, and highly dispersed species. The absence of any peaks due to Eu_2O_3 indicate that the Eu_2O_3 species are either amorphous and/or small (<3 nm) in size such that they are below the detection limits of the instrument. The unit cell parameters, *a*, and *c*, and the unit cell volumes were also calculated and the results are shown in Table 1. It can be noted that the unit cell volumes of the Eu-TiO_2 aerogel derived photocatalysts are lower than that of the pure titania, although the ionic radii of Eu^{3+}(0.0947 nm for 6-fold coordination) is much larger than that of Ti^{4+} (0.0605 nm for 6-fold coordination). Thus, we can infer that the Eu^{3+} ions are dispersed on the surface of the titania nanoparticle and probably exist as small clusters of europium oxide (<3 nm) since the solubility of Eu^{3+} ions in the TiO_2 lattice is limited because of its (Eu^{3+} ions) relatively large ionic radius. However, the trends in the unit cell volume, crystallite size, and Eu content appear to be independent, and do not necessarily follow any trends in accordance to our previous reports [2].

The crystallite sizes of the anatase phase were calculated using the Debye–Scherrer equation *i.e.* $D = 0.89\lambda/\beta\cos\theta$, where *D* is the crystallite size (Å), $\lambda = 1.5408$ Å, which is the wavelength of the Cu Kα radiation, β is the corrected full width at half maximum (FWHM) of the diffraction peak, and θ is the peak angle at which the diffraction occurs. This equation was applied to the d_{200} diffraction peak, and the results are summarized in Table 1. All the Eu-TiO_2 aerogel materials prepared in this study have crystallite sizes of TiO_2 in a fairly narrow range (9.1–10.7 ± 2 nm), which is very close to the threshold value of 10 nm. This is probably due to a combination of quantum size and surface stress effects. It has been reported that quantum size effects are more pronounced when the crystallite size of titania is less than 10 nm. Our results are in contrast to the results obtained by Li et al. [16] who observed an enhancement in the wt.% of the rutile to as high as 52% as the amount of Eu^{3+} ions were increased. Furthermore, the crystallite size of titania was also found to be about 3 times higher in their study compared to our study. This suggests that the supercritical drying method is a facile method for stabilizing titania crystallites of sizes ~10 nm. In general, there is a reduction in the lattice volume with decrease in crystallite size [14,41], with exception of the least Eu_2O_3 loaded aerogel, 0.72-Eu-TiO_2.

3.2. Physisorption studies

Fig. 2 shows the isotherms of the Eu-TiO_2 aerogels, and they are all representative of type IV isotherms according to the IUPAC classification. These isotherms are typical of mesoporous materials. At low relative pressures of P/P_0, the volume of nitrogen adsorbed varies linearly with the relative pressure. At moderate to high values, the amount of nitrogen physisorbed increases due to formation of multilayers and eventually capillary condensation occurs at high relative pressures of $P/P_0 \sim 1.0$. When the pore filling and the pore emptying mechanisms are different and occur separately (due to pore connectivity and network effects), the isotherms do not coincide and result in hysteresis. The hysteresis loops were of H3 classification (according to which the volume of nitrogen adsorbed do not level off at saturation values of the relative pressures near $P/P_0 \sim 1$) for the Eu-TiO_2 aerogels and these types of loops are characteristic of materials comprised of aggregates of plate-like particles that form slit like pores [42].

The pore size distributions were analyzed in order to understand the influence of supercritical drying on the pores of the aerogels. Fig. 2 displays the BJH pore distributions and indicates that the aerogel samples demonstrate uniformity of pores centered around 114 Å, with the broadest distribution exhibited by the aerogel with the least amount of Eu_2O_3 content, *i.e.* 0.72-Eu-TiO_2. The BET isotherm and BJH pore size distribution for the undoped

Table 2
Textural properties Eu-TiO_2 aerogels determined from N_2 physisorption analysis. The value preceding Eu-TiO_2 represents the wt.% of Eu_2O_3 loaded into the TiO_2.

Aerogel	S_{BET}[a] ($m^2\ g^{-1}$)	Pore volume ($cm^3\ g^{-1}$)	Average pore diameter (Å)	BJH pore diameter[b] (Å)	Band gap[c] (eV)
TiO_2	82.0	0.25	150	110	3.22
0.72-Eu-TiO_2	96.0	0.36	150	114	3.05
1.48-Eu-TiO_2	87.7	0.31	141	115	3.10
2.71-Eu-TiO_2	78.3	0.22	123	114	3.05
5.30-Eu-TiO_2	62.1	0.23	146	114	3.10

[a] Surface area determined by applying Brunauer–Emmett–Teller (BET) equation to a relative pressure (P/P_0) range of 0.05–0.35 of the adsorption isotherm.
[b] Pore diameter is calculated from the Barrett–Joyner–Halenda (BJH) equation using the desorption isotherm.
[c] Band gap energies estimated from Kubelka–Munk derived Tauc plots.

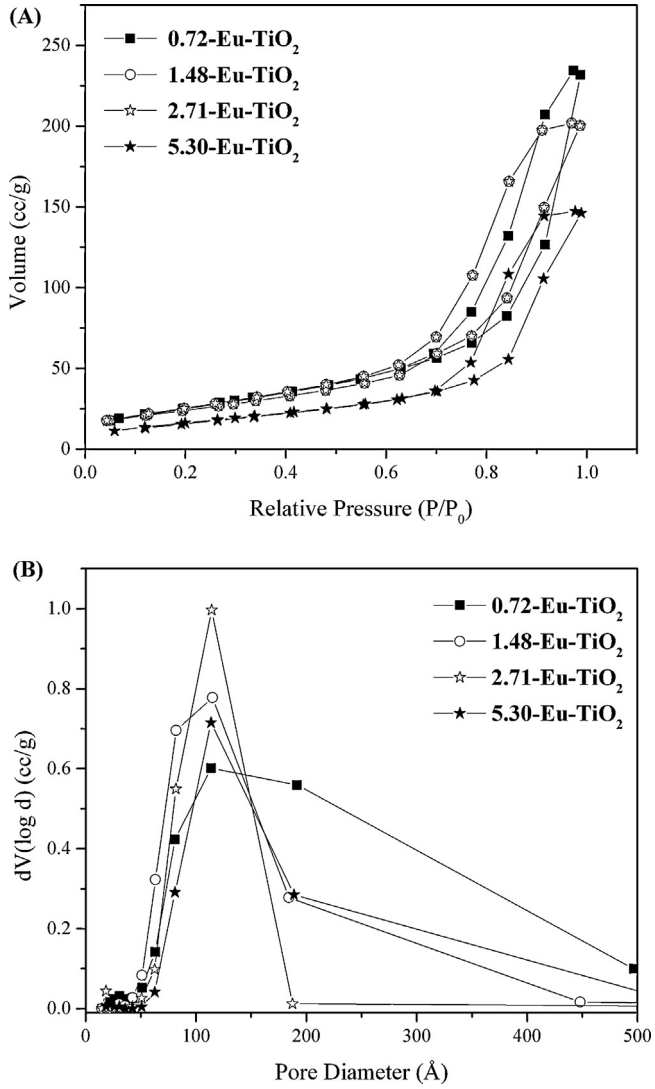

Fig. 2. (A) N_2 isotherms and (B) pore size distribution plots of Eu-TiO_2 aerogels. The value preceding Eu-TiO_2 represents the wt.% of Eu_2O_3 loaded into the TiO_2.

TiO_2 aerogel are shown in Fig. S1, and exhibit profiles similar to that of the Eu-TiO_2 aerogels. The isotherm of TiO_2 aerogel shows that the adsorption and desorption do not coincide at low relative pressures indicating presence of some micropores and/or strong adsorbate–adsorbent interactions. Comprehensive data of the textural properties obtained from the N_2 physisorption analysis at 77 K are summarized in Table 2. The aerogels exhibited surface areas ranging from 62 to 96 $m^2\ g^{-1}$ and appear to decrease with increased doping amounts of Eu_2O_3. The average pore diameters of the aerogels are greater than 140 Å on average, indicating that the pores are in the mesoporous range. The BJH pore diameters of the Eu-TiO_2 photocatalysts are identical suggesting the high dispersion of the small Eu_2O_3 clusters on the titania surface.

3.3. Transmission electron microscopy (TEM)

The TEM micrographs of a representative aerogel, 0.72-Eu-TiO_2 are shown in Fig. 3 for two different magnifications. The low magnification in Fig. 3A suggests the presence of porous particles with dark spots from high density electrons probably due to Eu_2O_3. Fig. 3B is a high magnification micrograph that exhibits large particle size distribution in the estimated range of 6–33 nm in diameter. The corresponding electron diffraction pattern is shown as an inset and indicates that the material is crystalline. This observation is consistent with the XRD analysis that exhibits diffraction patterns of crystalline anatase phase only.

3.4. Scanning electron microscopy (SEM) studies

Fig. 4 shows the scanning electron micrographs for a representative aerogel, 0.72-Eu-TiO_2. The higher magnification microimage in Fig. 4A shows smaller fiber-like particles on the surface which may be the europium oxide (Eu_2O_3). The particles may cluster together to form fairly large non-uniform agglomerates of irregular shapes as observed in the lower magnification image displayed in Fig. 4B. The aerogel agglomerates are estimated to range in sizes from 3 to 136 μm.

3.5. UV–vis diffuse reflectance spectroscopy (DRS) studies

Diffuse reflectance spectroscopy (DRS) was used to calculate the optical band gap of the aerogel materials. The DR spectra and corresponding Kubelka–Munk function derived Tauc plots are shown in Fig. 5A and B respectively, and were used to estimate the band gap energy by extrapolating the linear portion of the spectra to $[K \times E]^{1/2} = 0$. All samples exhibited a lower band gap energy compared to that of anatase TiO_2, which was estimated to be 3.2 eV. The band gap energies for the metal-oxide aerogels ranged from 3.05 to 3.10 eV. The spectrum of titania exhibits a similar profile with the absorption edge achieved at ~420 nm. The strong absorption at 300 nm is attributed to the excitation of electrons from the valence band to the conduction band of titania suggesting that the titania is octahedrally coordinated (Fig. S2A and S2B). Incorporation of rare earth metal ions such as Eu^{3+} leads to a slight shift in the onset of absorption. This may be attributed to the formation of sub-bandgap states that lie below the conduction band edge of titania. Thus, electronic states are inserted into the bandgap from 4f electrons from Eu^{3+} that lie closer to the lower edge of the conduction band of titanium dioxide. These sub-bandgap states may trap electrons and minimize charge-carrier recombination. In addition, it is noted that the absorbance of the photocatalysts in the UV range (200–350 nm) range for the 0.75-Eu-TiO_2 and 1.48-Eu-TiO_2 samples are similar; however on increasing the loading, the samples 2.71-Eu-TiO_2 and

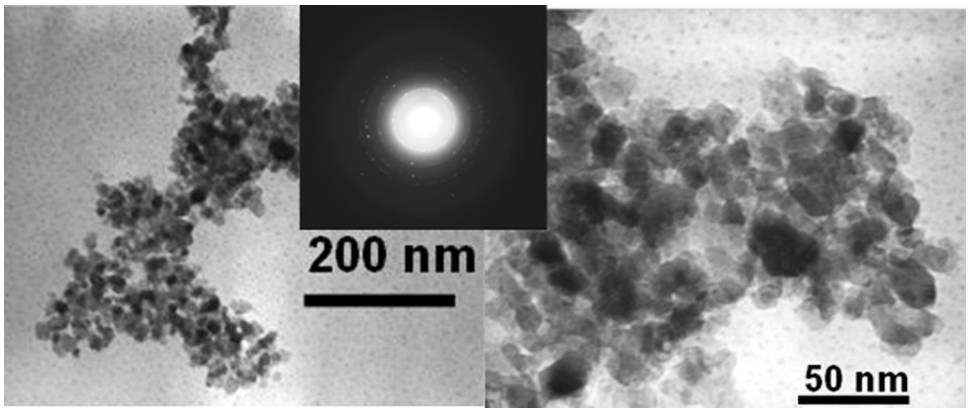

Fig. 3. TEM images of 0.72-Eu-TiO_2 of the least Eu_2O_3 loading at different magnifications shown as a representative for the aerogels prepared in this study. The image in the middle shows the electron diffraction pattern, depicting the crystalline nature of the aerogel.

5.30-Eu-TiO_2 show far lower absorbance. This may indicate that the europium oxide clusters that are formed in these two samples are effectively occluded in the pores of the titanium dioxide such that they are "screened" by the absorbance due to titanium dioxide particles. Evidence for this comes from the pore volumes of these materials. The pore volumes of 0.75-Eu-TiO_2 and 1.48-Eu-TiO_2 samples are fairly close whereas there is a sharp drop in the pore volumes of 2.71-Eu-TiO_2 and 5.30-Eu-TiO_2 suggesting that the europium oxide particles are occluded in the pores of titania, thus reducing the pore volumes.

3.6. Photoluminescence spectroscopy (PL) studies

Photoluminescence spectroscopy (PL) was carried out to investigate the electronic properties of the Eu-TiO_2 aerogels. Anatase TiO_2 nanoparticles are known to exhibit an emission band in the region of 360–550 nm on UV excitation at room temperature. In this study, the materials were first excited at 385 nm and a broad emission was observed in the range of 400–550 nm (Fig. 6A), which could be attributed to the band edge free excitons in TiO_2 [43,44]. The difference in intensities may be due to varying amounts of defect sites into which excitons are trapped and recombine.

Upon excitation of the Eu-TiO_2 aerogels at 465 nm (wavelengths longer than the absorption of TiO_2), characteristic peaks that correspond to radiative relaxations (4f–4f transitions) from the $^5D_0$ level to low-lying Russell-Saunders multiplet levels of Eu^{3+} activators, ^5F_j ($j = 1, 2, 3, 4$) are observed in the 500–720 nm range. Under our experimental conditions, peaks are observed at 594, 613, 652, and 700 nm that are attributed to $^5D_0 \rightarrow {}^7F_1$, $^5D_0 \rightarrow {}^7F_2$, $^5D_0 \rightarrow {}^7F_3$, and $^5D_0 \rightarrow {}^7F_4$ transitions, respectively. The $^5D_0 \rightarrow {}^7F_1$ and the $^5D_0 \rightarrow {}^7F_2$ lines arise from the magnetic dipole transition and electric dipole transitions respectively. These observations are consistent with those observed in previous reports for europium doped titania materials [14,22,37,45–48]. Some of the peaks exhibit broadening which may be indicative of the presence of detectable amorphicity in the oxide environment [48] or high disorder of the crystalline environment [49]. The most intense emission band at 613 nm due to the $^5D_0 \rightarrow {}^7F_2$ transition appears to be proportional to amount of europium ions present in the materials suggesting efficient non-radiative energy transfer from the TiO_2 host to Eu^{3+} ions. The energy transfer mode is defect mediated. According to this model, absorption of UV light by titania causes energy to be relaxed to the defect states. Since, the defect energy levels of titania are higher than that of the Eu^{3+} ions (emitting state of $^5D_0$), energy is transferred from TiO_2 to Eu^{3+}, resulting in photoluminescence. The defects in titania could be oxygen vacancies, interstitial Ti^{4+} ions *etc.*

3.7. X-ray photoelectron spectroscopy (XPS) studies

XPS was used to further investigate the oxidation state of europium species present in the aerogel materials. Fig. 7 shows the Eu 4d XPS spectra for the 5.30-Eu-TiO_2 sample after calcination. The survey spectra (not shown) indicated the presence of elemental Eu, Ti, O, and C. The carbon detected in these materials may be primarily due to adventitious carbon. The absence of nitrogen was confirmed, suggesting the complete decomposition of europium nitrate during the calcination conditions of 550 °C as described earlier in the manuscript. The Eu 4d region of the photoelectron spectrum consists of two peaks corresponding to the $4d_{5/2}$

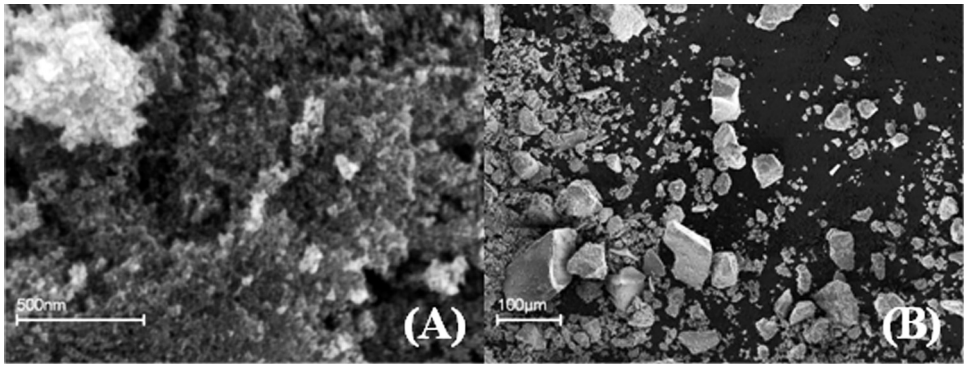

Fig. 4. SEM images of 0.72-Eu-TiO_2 at different magnifications (A) 0.5 μm and (B) 100 μm shown as a representative for the aerogels prepared in this study.

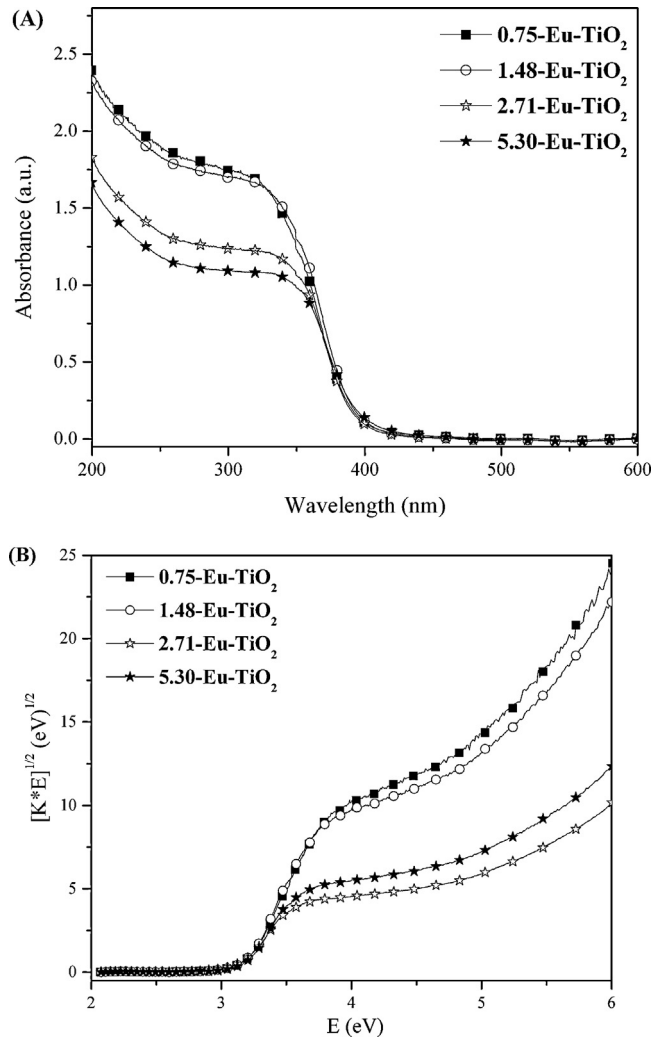

Fig. 5. (A) UV–vis diffuse reflectance spectra and (B) corresponding Tauc plots of Eu-TiO_2 aerogels. The value preceding Eu-TiO_2 represents the wt.% of Eu_2O_3 loaded into the TiO_2.

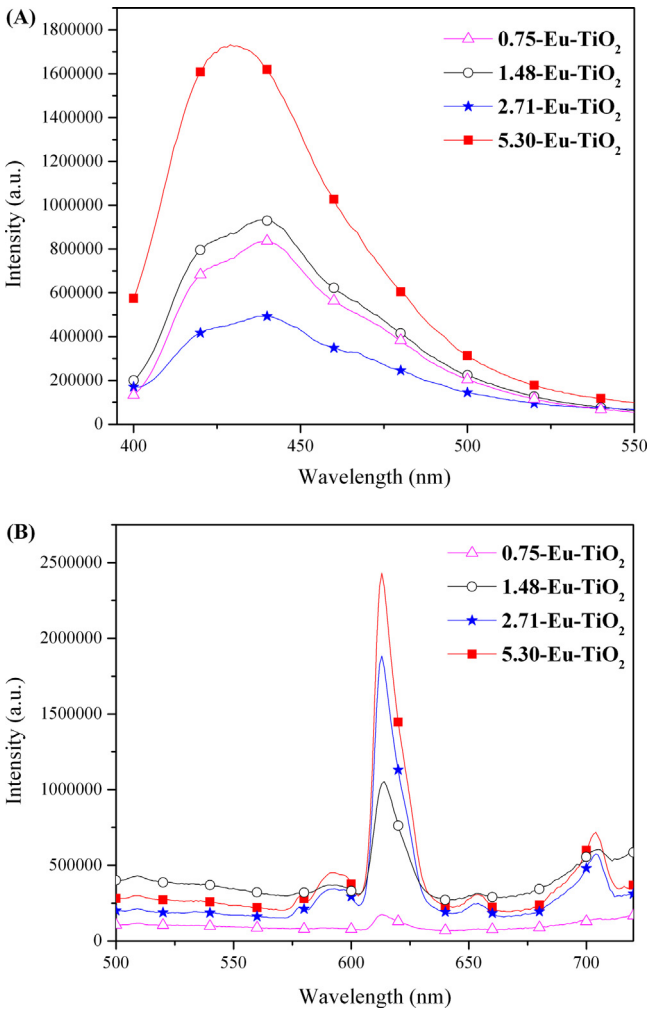

Fig. 6. Photoluminescence emission spectra of Eu-TiO_2 aerogels (A) under excitation of 385 nm and observed in the 400–550 nm range, and (B) under excitation of 465 nm and observed in the 500–720 nm range. The value preceding Eu-TiO_2 represents the wt.% of Eu_2O_3 loaded into the TiO_2.

and $4d_{3/2}$ transitions with a ratio of 3 to 2. The peaks are located at 135.2 and 140.7 eV respectively and are ascribed to the presence of Eu_2O_3. These results are consistent with previous reports [12,50].

3.8. Photocatalytic performance of Eu-TiO_2 aerogels

The photocatalytic performance of the Eu-TiO_2 aerogels was elucidated by using the degradation of salicylic acid as a model pollutant. The loss in intensity of the peak at 296 nm of the UV–vis spectra was monitored, and used to calculate the amount of salicylic degraded after UV irradiation in the presence of aerogel photocatalyst for a specified period. Fig. 8 shows the UV–vis spectra of the 0.72 wt.% Eu_2O_3 doped TiO_2 (0.72-Eu-TiO_2), used as a representative aerogel after being irradiated at 0, 30, 45, and 60 min. It is evident that the amount of salicylic acid degraded decreases with irradiation time as observed by the decrease in intensity of the peak at 296 nm. This trend was observed for all degraded solution samples of the other photocatalysts. The salicylic acid degradation activity using undoped TiO_2, 0.72, 1.48, 2.71 and 5.30-Eu-TiO_2 aerogels were determined to be 4.4 ± 2, 84.8 ± 4, 78.1 ± 4, 79.6 ± 4, and 100% after 60 min of UV irradiation. These results are consistent with the TOC data that indicates a reduction in total organic carbon due to photocatalytic degradation of salicylic acid.

The origin of the degradation efficiencies is often debated for several photocatalytic systems and is dependent on several factors that may include preparation and drying methods, calcination temperatures, crystallinity, dispersion, adsorption, particle (or crystallite) sizes, and crystal structure or phases. Since the photocatalytic efficiency is a synergetic function of several factors, it is challenging to model all of these factors to design an ideal photocatalyst. However, the results of this study forms a basis in guiding future research using rare-earth doped photocatalysts. In this work, the influence of adsorption capacity on the photocatalytic activity was investigated. The dark adsorption experiments over a 6 h period indicated that negligible amounts (<1 $\mu mol\, g^{-1}$) of salicylic acid molecules were adsorbed by undoped TiO_2 aerogel. Under similar experimental conditions, the 0.72, 1.48, 2.71, 5.30-Eu-TiO_2 photocatalysts exhibited adsorption amounts of 33.5, 35.3, 33.2, and 31.8 $\mu mol\, g^{-1}$ of salicylic acid, which are significantly higher capacities to that compared to the undoped TiO_2 (Fig. 9). Thus the low activity of undoped TiO_2 aerogel (4.4%) may be attributed to the low adsorption capacity of the photocatalyst. In turn, the enhanced activities of Eu-TiO_2 photocatalysts may be due to higher adsorption capacities. The amounts adsorbed by the doped materials are in somewhat similar range with the 5.30-Eu-TiO_2 photocatalyst showing complete degradation of salicylic acid. This indicates that, apart from adsorption, there could be other

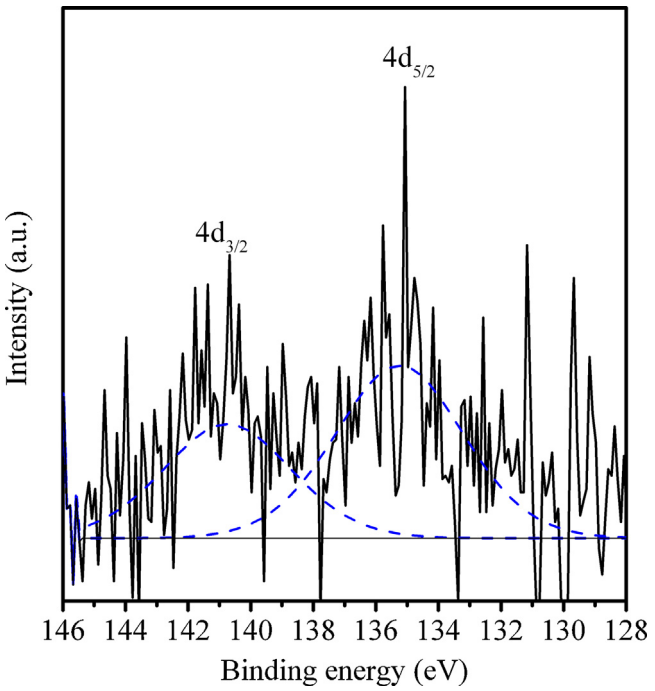

Fig. 7. XPS spectrum showing a representative photocatalyst of highest Eu_2O_3 doped TiO_2 aerogels, 5.30-Eu-TiO_2.

physico-chemical factor(s) that is influencing the resultant photocatalytic activity. Since, the crystallite sizes of titania in the Eu-TiO_2 photocatalysts are in the same ranges of $9.1–10.7 \pm 2.0$ nm, the crystallite size of titania cannot be a factor affecting the photocatalytic activities. The specific surface areas of titania decrease with increase in Eu content and hence any effects due to surface area is marginal.

In order to verify the role of reactive oxidation species (ROS), the degradation of salicylic acid was investigated by carrying out scavenging experiments. The most and the least active Eu-TiO_2 photocatalysts were used as representative photocatalysts. N_2 purged experiments were carried out to establish the role of molecular oxygen on the degradation of salicylic acid and UV–vis spectra results are summarized in Fig. S3. The presence of N_2 significantly reduces the photocatalytic activity to 25% for 5.30-Eu-TiO_2 photocatalyst which suggests that the presence of O_2 is crucial factor for the formation of superoxide radicals ($O_2^{\bullet-}$), from which highly reactive •OH radicals may be generated. Since •OH radicals are believed to be the most reactive oxidative species responsible for photocatalysis, •OH trapping experiments were carried out to estimate the formation of •OH under these UV light irradiation conditions and confirm their role in the degradation of salicylic acid. Fig. 10 shows a plot of 2-hydroxyterephthalic acid *vs.* time for the photocataytically less efficient 1.48-Eu-TiO_2 and the more active 5.30-Eu-TiO_2. Within the first 20 min of the reaction, it is evident that the amount of •OH generated is lower for 1.48-Eu-TiO_2 due to more charge-carrier recombination, and this produces lesser amounts of 2-hydroxyterephthalic acid as compared to the 5.30-Eu-TiO_2 photocatalyst. It is observed that the •OH formation is maintained even after 60 min in the 5.30-Eu-TiO_2 photocatalyst. Since the ionic radii of Eu^{3+} is higher than that of Ti^{4+}, it is not possible for Eu^{3+} to substitute for Ti^{4+} in the titania lattice. Thus, it is most likely that the rare earth exist as oxides that are well dispersed on the titania matrix as discussed previously. It is possible that some of the Ti^{4+} can substitute in the rare earth metal oxide, Eu_2O_3. Since, Eu ions are trivalent, substitution by altervalent cation such as Ti^{4+}, will lead to a charge imbalance. The excess charges may be balanced

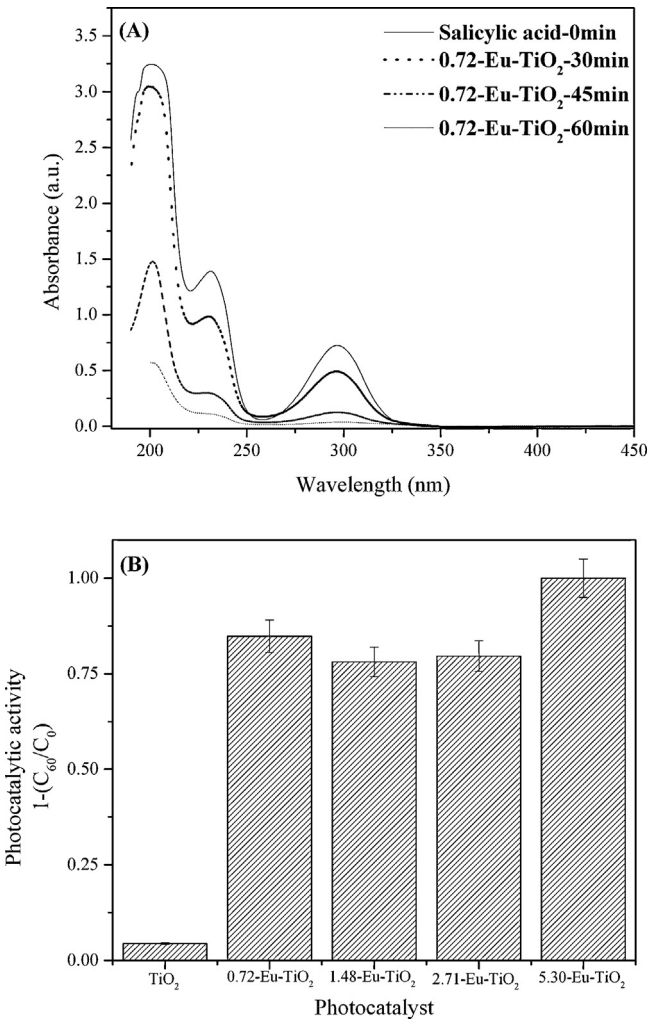

Fig. 8. Absorption spectra of salicylic acid remaining after degradation using 0.72-Eu-TiO_2 at different time intervals. The value preceding Eu-TiO_2 represents the wt.% of Eu_2O_3 loaded into the TiO_2.

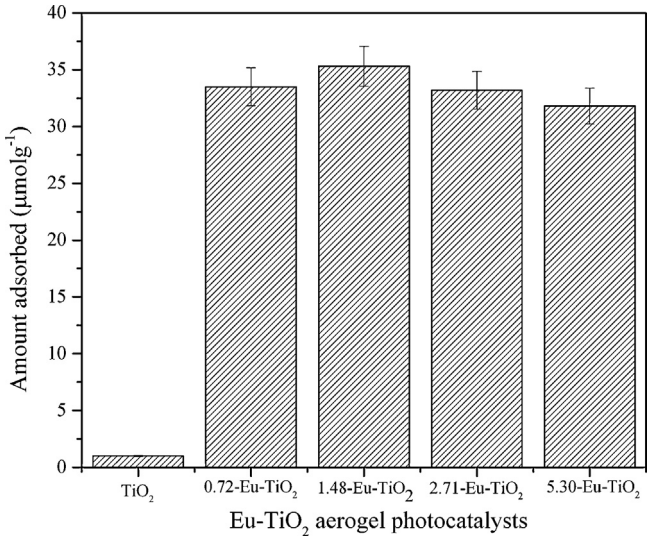

Fig. 9. Plots summarizing amount ($\mu mol\, g^{-1}$) of salicylic acid adsorbed in the dark after 6 h. The value preceding Eu-TiO_2 represents the wt.% of Eu_2O_3 loaded into the TiO_2.

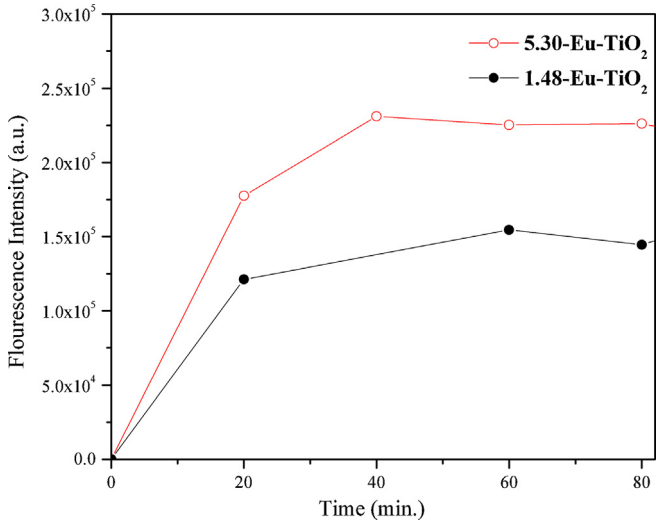

Fig. 10. Plot showing fluorescence intensity against time that compares the amount of •OH radicals formed from photocatlaytically less efficient 1.48-Eu-TiO_2 and the more active 5.30-Eu-TiO_2. The value preceding Eu-TiO_2 represents the wt.% of Eu_2O_3 loaded into the TiO_2.

by adsorption of water, *i.e. i.e.* hydroxyl groups. Thus, the addition of Eu^{3+} can lead to an enhancement in surface hydroxyl groups. If this is true, the surface hydroxyl groups can react with the photogenerated holes to form hydroxyl radicals and initiate the photocatalytic reaction. This implies that the europium oxide trap electrons from TiO_2, which are then transferred to the dissolved oxygen to eventually form more reactive oxidative species that degrade salicylic acid more efficiently. Similar trends were observed for the other series of photocatalysts. Thus, the presence of more •OH radicals invoked by the appropriate amounts of dispersed europium ions is responsible for the slightly enhanced activity in 5.30-Eu-TiO_2 compared to the rest of the samples.

4. Conclusions

Synthetic strategies for the preparation of rare earth europium oxide doped TiO_2 aerogel photocatalysts were developed for the *first* time and show enhanced photocatalytic activities compared with undoped TiO_2 from the degradation of salicylic acid. The sol–gel method provides a convenient method to prepare doped TiO_2 photocatalysts. One of the objectives of this study was to explore the influence of the supercritical drying method and the Eu_2O_3 content on the physicochemical properties and the resultant photocatalytic activity of the aerogels obtained. We demonstrate that the photocatalytic activity was dependent on the presence of the active anatase phase. In addition, well dispersed europium dopants may lead to the formation of surface oxygen defects that can serve as trap states and minimizes recombination of charge carriers. The availability of electrons facilitates the formation of •OH radicals that are crucial for the photodegradation process as evidence by the fluorescence scavenging experiments. Future studies will explore and compare the photocatalytic efficiencies of other rare-earth metal ions such as La^{3+}, Nd^{3+}, Pr^{3+} *etc.* with Eu^{3+}.

Acknowledgements

We extend sincere gratitude to NSF-CHE-0619190, NSF-CHE-0722632, NSF-EPS-0903804, DE-EE0000270, and State of SD for funding this project. We are thankful Dr. S. P. Ahrenkiel for TEM and Dr. Glen Stone for SEM measurements.

Appendix A. Supplementary data

Supplementary data associated with this article can be found, in the online version, at http://dx.doi.org/10.1016/j.jphotochem.2013.07.006.

References

[1] X. Chen, S.S. Mao, Titanium dioxide nanomaterials: synthesis, properties, modifications, and applications, Chemical Reviews 107 (2007) 2891–2959.
[2] K.T. Ranjit, I. Willner, S.H. Bossmann, A.M. Braun, Lanthanide oxide-doped titanium dioxide photocatalysts: novel photocatalysts for the enhanced degradation of p-chlorophenoxyacetic acid, Environmental Science and Technology 35 (2001) 1544–1549.
[3] J. Lin, J.C. Yu, An investigation on photocatalytic activities of mixed TiO_2-rare earth oxides for the oxidation of acetone in air, Journal of Photochemistry and Photobiology A: Chemistry 116 (1998) 63–67.
[4] I. Cacciotti, A. Bianco, G. Pezzotti, G. Gusmano, Synthesis, thermal behaviour and luminescence properties of rare earth-doped titania nanofibers, Chemical Engineering Journal 166 (2011) 751–764.
[5] A.C. Pierre, G.M. Pajonk, Chemistry of aerogels and their applications, Chemical Reviews 102 (2002) 4243–4266.
[6] N. Hüsing, U. Schubert, Aerogels – airy materials: chemistry, structure, and properties, Angewandte Chemie International Edition 37 (1998) 22–45.
[7] D.R. Rolison, B. Dunn, Electrically conductive oxide aerogels: new materials in electrochemistry, Journal of Materials Chemistry 11 (2001) 963–980.
[8] N. Hüsing, F. Schwertfeger, W. Tappert, U. Schubert, Influence of supercritical drying fluid on structure and properties of organically modified silica aerogels, Journal of Non-Crystalline Solids 186 (1995) 37–43.
[9] D.C.M. Dutoit, M. Schneider, A. Baiker, Titania-silica mixed oxides. I. Influence of sol–gel and drying conditions on structural properties, Journal of Catalysis 153 (1995) 165–176.
[10] Y.V. Kolen'ko, A.V. Garshev, B.R. Churagulov, S. Boujday, P. Portes, C. Colbeau-Justin, Photocatalytic activity of sol–gel derived titania converted into nanocrystalline powders by supercritical drying, Journal of Photochemistry and Photobiology A: Chemistry 172 (2005) 19–26.
[11] M. Schneider, A. Baiker, Titania-based aerogels, Catalysis Today 35 (1997) 339–365.
[12] Z. Liu, J. Zhang, B. Han, J. Du, T. Mu, Y. Wang, Z. Sun, Solvothermal synthesis of mesoporous Eu_2O_3–TiO_2 composites, Microporous and Mesoporous Materials 81 (2005) 169–174.
[13] X.A. Feng, L. Yang, N.C. Zhang, Y.L. Liu, A facile one-pot hydrothermal method to prepare europium-doped titania hollow phosphors and their sensitized luminescence properties, Journal of Alloys and Compounds 506 (2010) 728–733.
[14] P. Ghosh, A. Patra, Influence of surface coating on physical properties of TiO_2/Eu^{3+} nanocrystals, Journal of Physical Chemistry C 111 (2007) 7004–7010.
[15] S. Jeon, P.V. Braun, Hydrothermal synthesis of Er-doped luminescent TiO_2 nanoparticles, Chemistry of Materials 15 (2003) 1256–1263.
[16] J.-G. Li, X. Wang, K. Watanabe, T. Ishigaki, Phase structure and luminescence properties of Eu^{3+}-doped TiO_2 nanocrystals synthesized by Ar/O_2 radio frequency thermal plasma oxidation of liquid precursor mists, Journal of Physical Chemistry B 110 (2005) 1121–1127.
[17] W. Luo, R. Li, G. Liu, M.R. Antonio, X. Chen, Evidence of trivalent europium incorporated in anatase TiO_2 nanocrystals with multiple sites, Journal of Physical Chemistry C 112 (2008) 10370–10377.
[18] R.S. Ningthoujam, V. Sudarsan, R.K. Vatsa, R.M. Kadam, Jagannath, A. Gupta, Photoluminescence studies on Eu doped TiO_2 nanoparticles, Journal of Alloys and Compounds 486 (2009) 864–870.
[19] E. Setiawati, K. Kawano, T. Tsuboi, H.J. Seo, Studies on thermal migration of Eu ion doped into TiO_2 nanoparticles, Japanese Journal of Applied Physics 47 (2008) 4651–4657.
[20] Y.R. Wang, Y.J. Guo, G.J. Wang, F. Wang, Investigation of Eu-doped mesoporous titania phosphor with enhanced luminescence, Journal of Nanoscience and Nanotechnology 11 (2011) 3162–3170.
[21] Q.G.D. Zeng, Z.J. Zhang, Z.M. Synthesis, structure and optical properties of Eu^{3+}/TiO_2 nanocrystals at room temperature, Journal of Luminescence 118 (2006) 301–307.
[22] C.M. Leroy, H.F. Wang, A. Fargues, T. Cardinal, V. Jubera, M. Treguer-Delapierre, C. Boissiere, D. Grosso, C. Sanchez, B. Viana, F. Pelle, Emission-photoactivity cross-processing of mesoporous interfacial charge transfer in Eu^{3+} doped titania, Physical Chemistry Chemical Physics 13 (2011) 11878–11884.
[23] D. Chen, Q. Zhu, Z. Lv, X. Deng, F. Zhou, Y. Deng, Microstructural and photocatatlytic properties of Eu-doped mesporous titanium dioxide nanopaticles by sol–gel method, Materials Research Bulletin 47 (2012) 3129–3134.
[24] L. Diamandescu, F. Vasiliu, D. Tarabasanu-Mihaila, M. Feder, A.M. Vlaicu, C.M. Teodorescu, D. Macovei, I. Enculescu, V. Parvulescu, E. Vasile, Structural and photocatalytic properties of iron- and europium-doped TiO_2 nanoparticles obtained under hydrothermal conditions, Materials Chemistry and Physics 112 (2008) 146–153.
[25] Z.M. El-Bahy, A.A. Ismail, R.M. Mohamed, Enhancement of titania by doping rare earth for photodegradation of organic dye (direct blue), Journal of Hazardous Materials 166 (2009) 138–143.

[26] R.C. Hsiao, N.S. Arul, D. Mangalaraj, R.S. Juang, Influence of Eu^{3+} doping on the degradation property of TiO_2 nanostructures, Journal of Optoelectronics and Advanced Materials 12 (2010) 193–198.
[27] K.T. Ranjit, H. Cohen, I. Willner, S. Bossmann, A.M. Braun, Lanthanide oxide-doped titanium dioxide: effective photocatalysts for the degradation of organic pollutants, Journal of Materials Science 34 (1999) 5273–5280.
[28] S. Matsuo, N. Sakaguchi, K. Yamada, T. Matsuo, H. Wakita, Role in photocatalysis and coordination structure of metal ions adsorbed on titanium dioxide particles: a comparison between lanthanide and iron ions, Applied Surface Science 228 (2004) 233–244.
[29] H.X. Shi, T.Y. Zhang, H.L. Wang, Preparation, photocatalytic activity of La^{3+} and Eu^{3+} co-doped TiO_2 nanoparticles: photo-assisted degradation of methylene blue, Journal of Rare Earths 29 (2011) 746–752.
[30] Y. Zhang, H. Zhang, Y. Xu, Y. Wang, Europium doped nanocrystalline titanium dioxide: preparation, phase transformation and photocatalytic properties, Journal of Materials Chemistry 13 (2003) 2261–2265.
[31] V. Štengl, S. Bakardjieva, N. Murafa, Preparation and photocatalytic activity of rare earth doped TiO_2 nanoparticles, Materials Chemistry and Physics 114 (2009) 217–226.
[32] Y. Xie, C. Yuan, Characterization and photocatalysis of Eu^{3+}–TiO_2 sol in the hydrosol reaction system, Materials Research Bulletin 39 (2004) 533–543.
[33] Y.B. Xie, C.W. Yuan, Transparent TiO_2 sol nanocrystallites mediated homogeneous-like photocatalytic reaction and hydrosol recycling process, Journal of Materials Science 40 (2005) 6375–6383.
[34] Z.L. Xu, Q.J. Yang, C. Xie, W.J. Yan, Y.G. Du, Z.M. Gao, J.H. Zhang, Structure, luminescence properties and photocatalytic activity of europium doped-TiO_2 nanoparticles, Journal of Materials Science 40 (2005) 1539–1541.
[35] Q.J. Yang, Z.L. Xu, C. Xie, B.Y. Xue, Y.G. Du, J.H. Zhang, Effect of Eu^{3+} doping on the photocatalytic activity of nanoparticles TiO_2, Chemical Journal of Chinese Universities – Chinese 25 (2004) 1711–1714.
[36] S.H. Yao, C.C. Sui, Z.L. Shi, Preparation and characterization of visible-light-driven europium doped mesoporous titania photocatalyst, Journal of Rare Earths 29 (2011) 929–933.
[37] M. Pal, U. Pal, J.M. Jimenez, F. Perez-Rodriguez, Effects of crystallization and dopant concentration on the emission behavior of TiO_2:Eu nanophosphors, Nanoscale Research Letters 7 (2012) 1.
[38] A.S. Weber, A.M. Grady, R.T. Koodali, Lanthanide modified semiconductor photocatalysts, Catalysis Science and Technology 2 (2012) 683–693.
[39] S. Utamapanya, K.J. Klabunde, J.R. Schlup, Nanoscale metal oxide particles/clusters as chemical reagents. Synthesis and properties of ultrahigh surface area magnesium hydroxide and magnesium oxide, Chemistry of Materials 3 (1991) 175–181.
[40] B. Sun, P.G. Smirniotis, P. Boolchand, Visible light photocatalysis with platinized rutile TiO_2 for aqueous organic oxidation, Langmuir 21 (2005) 11397–11403.
[41] H. Zhang, J.F. Banfield, Understanding polymorphic phase transformation behavior during growth of nanocrystalline aggregates: insights from TiO_2, Journal of Physical Chemistry B 104 (2000) 3481–3487.
[42] M. Kruk, M. Jaroniec, Gas adsorption characterization of ordered organic–inorganic nanocomposite materials, Chemistry of Materials 13 (2001) 3169–3183.
[43] J. Yu, L. Yue, S. Liu, B. Huang, X. Zhang, Hydrothermal preparation and photocatalytic activity of mesoporous Au–TiO_2 nanocomposite microspheres, Journal of Colloid and Interface Science 334 (2009) 58–64.
[44] J. Yu, L. Qi, M. Jaroniec, Hydrogen production by photocatalytic water splitting over Pt/TiO_2 nanosheets with exposed (0 0 1) facets, Journal of Physical Chemistry C 114 (2010) 13118–13125.
[45] K.L. Frindell, M.H. Bartl, M.R. Robinson, G.C. Bazan, A. Popitsch, G.D. Stucky, Visible and near-IR luminescence via energy transfer in rare earth doped mesoporous titania thin films with nanocrystalline walls, Journal of Solid State Chemistry 172 (2003) 81–88.
[46] P. Aihua, X. Erqing, J. Changwen, J. Ran, L. Hongfeng, Photoluminescence properties of TiO_2:Eu^{3+} thin films deposited on different substrates, Materials Letters 59 (2005) 3866–3869.
[47] S. Sandoval, J. Yang, J.G. Alfaro, A. Liberman, M. Makale, C.E. Chiang, I.K. Schuller, A.C. Kummel, W.C. Trogler, Europium-doped TiO_2 hollow nanoshells: two-photon imaging of cell binding, Chemistry of Materials 24 (2012) 4222–4230.
[48] K.L. Frindell, M.H. Bartl, A. Popitsch, G.D. Stucky, Sensitized luminescence of trivalent europium by three-dimensionally arranged anatase nanocrystals in mesostructured titania thin films, Angewandte Chemie 114 (2002) 1001–1004.
[49] D. Falcomer, M. Daldosso, C. Cannas, A. Musinu, B. Lasio, S. Enzo, A. Speghini, M. Bettinelli, A one-step solvothermal route for the synthesis of nanocrystalline anatase TiO_2 doped with lanthanide ions, Journal of Solid State Chemistry 179 (2006) 2452–2457.
[50] Y. Uwamino, T. Ishizuka, H. Yamatera, X-ray photoelectron spectroscopy of rare-earth compounds, Journal of Electron Spectroscopy and Related Phenomena 34 (1984) 67–78.